Pd immobilized Schiff-base double layer macrocycle: synthesis, structures, peroxidase mimic activity and antibacterial performance

Kuiyuan Wang,[a] Kai Chen,[b] Timothy J. Prior,[a] Xing Feng,[c] and Carl Redshaw[a]*

[a] Department of Chemistry, University of Hull, Hull, HU6 7RX, U.K.

[b] Collaborative Innovation Center of Atmospheric Environment and Equipment Technology, Jiangsu Key Laboratory of Atmospheric Environment Monitoring and Pollution Control, School of Environmental Science and Engineering, Nanjing University of Information Science & Technology, Nanjing 210044, P. R. China.

[c] School of Chemistry and Chemical Engineering, Department of Chemistry, Harbin Institute of Technology, Harbin 150040, P. R. China.

ABSTRACT

Di-, tri- and tetra-aldehydes have been employed to access new [2+2] [2+3] and [2+4] double layer Schiff-base macrocycles. The [2+3] compound has been used for the immobilization of Pd, and the resulting composite has been employed as a peroxidase-like mimetic using 3,3',5,5'-tetramethylbenzidine (TMB) as the substrate; the optimum conditions together with the catalytic kinetics of the enzyme-like activity is discussed. Based on the peroxidase-like catalytic activity,

the Pd@Schiff base composite was found to exhibit excellent bactericidal activity against both Escherichia coli (Gram-negative bacterium) and Staphylococcus aureus (Gram-positive bacterium) in the presence of a relatively low concentrations of H_2O_2. Furthermore, cytotoxicity measurements illustrate the biosafety of the Pd composite. The above-mentioned findings have the potential to guide the innovation of new Pd-based composites as enzyme-mimetics and antibacterial materials.

KEYWORDS: Schiff-base macrocycle, Antibacterial, Pd composite; Peroxidase-like activity.

INTRODUCTION

Enzymes are biocatalysts produced in living cells,[1] which can catalyze various biological and chemical processes efficiently by reducing their activation energy. However, the limitations of natural enzymes, such as high isolation costs, low stability and storage difficulties, have led to the emergence of various artificial enzymes. Recently, varieties of artificial enzymes have been developed, such as peroxidase,[2] catalase,[3] superoxide dismutase,[4] lipase,[5] etc., whilst Horseradish peroxidase (HRP) has become a hot topic of research because of its diverse applications. Over the last decade, increasing numbers of materials have been utilized as peroxidase-like mimetics, for example, metal oxides,[6] precious metals,[7] quantum dots,[8] MOFs,[9] composites[10] and so on. Such systems have been widely applied in many fields such as analytical chemistry,[11] antibacterial[12] and in the degradation of dyes or other pollutants.[13] Given their ease of acquisition, high efficiency and stability, such artificial mimetics are of great interest.

Schiff-base macrocycles are considered as ''privileged ligands''[14] because of their ease of preparation, *i.e.* condensation between aldehydes and imines to form the "-RC=N-" linkage. This has led to Schiff-base chemistry receiving much attention over the years, and such compounds have been widely employed in luminescence sensing,[15] biomaterial,[16] catalytic chemistry,[17] and

soon. Of note is the discovery by Ni *et al* of a Schiff-base macrocyclic host that can serve as a probe for Cu^{2+} and Fe^{3+} ion sensing.[18] Schiff-base compounds can adopt a variety of structural types; macrocycles,[19] cages[20] and helices[21] are well established.

In recent years, interest in Pd-based heterogeneous catalysts has increased because of the wide range of potential applications together with their good reusability. For instance, palladium nanoparticles (Pd NPs) using an organic molecular cage as template have been synthesized and can be utilized as an efficient catalysts in Suzuki–Miyaura coupling reactions.[22] In 2017, Nasrollahzadeh *et al*. reported the synthesize of a GO/Pd nanocomposite that was found to be an excellent heterogeneous catalyst for degradation of dyes in the presence of $NaBH_4$.[23] Moreover, the incorporation of Pd and enzymes within porous Schiff-base molecular cages was reported by Jiang *et al*., and the resulting composite materials exhibited high efficiency in semi-heterogeneous chemoenzymatic catalysis.[24] In 2018, palladium (Pd) nanocrystals were found to display facet-dependent oxidase and peroxidase-like activities and distinct antibacterial activity against Gram-positive and Gram-negative bacteria.[25] Based on the above-mentioned reports, the demand for new Pd-based composites as functional materials has increased dramatically.

Despite the plethora of chemistry on Pd-based materials and Schiff bases, reports concerning the structures and properties of double layered Schiff-base macrocycles and their Pd metal composites, particularly systems exhibiting enzyme-like and bactericidal activity, are rare. Herein, we report a series of [2+2], [2+3] and [2+4] Schiff-base double layer macrocycles derived from 2,2'-ethylenedianiline. It is noteworthy that the [2+2] and [2+3] double layer macrocycles were synthesized in high yield via a one-pot procedure, whilst the [2+4] macrocycle was prepared in two steps and required the presence of a metal. For the first time, we report a Pd composite of a [2+3] double-layer macrocycle and investigate its enzyme-like activity and apply

it against the bacteria *Escherichia coli* (Gram-negative bacterium) and *Staphylococcus aureus* (Gram-positive bacterium) in the presence of a relatively low concentrations of H_2O_2.

EXPERIMENTAL

General

All the chemicals were purchased in reagent grade and were reacted without further purification. All syntheses were carried out under nitrogen using standard Schlenk techniques. All solvents were distilled and degassed prior to use. Toluene was refluxed over sodium, and dichloromethane was dried over calcium hydride. IR spectra were recorded using the Nicolet Avatar 360 FT-IR spectrometer; NMR spectra were recorded at room temperature on a Varian VXR 400 S spectrometer at 400 MHz. Elemental analyses were determined in Nanjing University of Information Science & Technology. Melting points were recorded using Stuart SPM 10 machine with a temperature range of ambient to 300 ℃. The mass spectra were recorded at the National Mass Spectrometry Service (Swansea). Deionized water purified by the Milli-Q water system (Millipore) was used in all the studies. Sodium alginate, Corning Transwell polyester membrane cell culture inserts (24-well plates) and T75 EasY flasks were purchased from Thermo Fisher Scientific (UK). DMEM, EMEM and Trypsin-EDTA solution were sourced from Gibco (UK). Media supplements were fetal bovine serum (FBS) (10% v/v, Labtech, Heathfield, UK). CellTiter 96® AQ ueous One Solution Cell Proliferation Assay (MTS assay), was sourced from Promega, Madison, used for mammalian cell viability measurement. Fluorescein diacetate (FDA) for cell viability test was purchased from Sigma-Aldrich. HaCaT cell line culture was purchased from AddexBio (T0020001). Hep-G2 cell line culture was purchased from Public Health England (PHE, Culture collection 85011430 Hep G2) cultured from growing cells. The American Type Culture Collection S. aureus subsp. aureus Rosenbach (ATCC 29213) and Escherichia coli (Migula) Castellani and Chalmers (ATCC 25922) were used in this work. All other chemicals

4

were of the analytical grade.

Synthesis of [(C$_6$H$_4$)$_2$-4-(CH)$_2$]$_2$[CH$_2$CH$_2$(2-C$_6$H$_4$N)$_2$]$_2$ (1)

4,4'-Biphenyldicarboxaldehyde (420.5 mg, 2.0 mmol) was dissolved in dichloromethane (25 mL), and 2,2'-ethylenedianiline (424.6 mg, 2.0 mmol) was dissolved in toluene (25 mL). The two solutions were mixed at room temperature without any stirring. Finally, 1 drop of trifluoroacetic acid was added to this solution as a catalyst for imine bond formation. Prolonged standing at room temperature for one week afforded egg-white colored prisms. Yield: 507 mg, 69.2%. IR (KBr, cm^{-1}): 2954 (s), 2923 (s), 2854 (s), 2726 (w), 1675 (w), 1624 (w), 1605 (w), 1590 (w), 1573 (w), 1552 (w), 1463 (s), 1377 (s), 1310 (m), 1205 (w), 1171 (w), 1153 (w), 1132 (w), 1003 (w), 969 (w), 938 (w), 886 (w), 857 (w), 817 (m), 753 (m), 722 (m). ^{1}H NMR (CD$_2$Cl$_2$): 8.47 (s, C*H*=N, 4H), 7.98-6.64 (s, Ar-*H*, 32H), 2.75 (s, -C*H*$_2$, 12H). MS (ES+): C$_{56}$H$_{44}$N$_4$ (sample dried *in-vacuo*) 773.4. Elemental analysis calculated for C$_{56}$H$_{44}$N$_4$ C 87.01, H 5.74, N 7.25%; found: C 86.98, H 5.91, N 7.09%. M. pt > 300 ºC.

Synthesis of [C$_6$H$_3$-1,3,5-(CH)]$_2$[CH$_2$CH$_2$(2-C$_6$H$_4$N)$_2$]$_3$·0.84CH$_2$Cl$_2$ (2)

1,3,5-Triformylbenzene (324.3 mg, 2.0 mmol) was dissolved in dichloromethane (25 mL) and 2,2'-ethylenedianiline (636.9 mg, 3.0 mmol) was dissolved in toluene (30 mL). The two solutions were mixed at room temperature without any stirring. Finally, 1 drop of trifluoroacetic acid was added to this solution as a catalyst for imine bond formation. Prolonged standing at room temperature for one week afforded egg-white colored prisms. Yield: 665 mg, 72.1%. IR (KBr, cm^{-1}): 2954 (s), 2923 (s), 2854 (s), 1629 (w), 1591 (w), 1537 (w), 1462 (s), 1377 (s), 1261 (s), 1141 (m), 1093 (s), 1019 (s), 976 (w), 864 (w), 801 (s), 754 (m), 723 (m), 683 (m). ^{1}H NMR (CD$_2$Cl$_2$): δ 8.44 (s, CH=N, 6H), 8.13-6.98 (s, Ar-H, 30H), 3.22 (s, -CH$_2$, 12H). ^{13}C NMR

(CD$_2$Cl$_2$): δ 157.05, 149.22 137.65, 130.61, 129.83, 127.23, 126.99, 117.79, 33.56, 33.0, 31.19, 30.61 ppm. MS (ES+): C$_{60}$H$_{48}$N$_6$ (sample dried *in-vacuo*) 853.4. Elemental analysis calculated for C$_{60}$H$_{48}$N$_6$ C 84.48, H 5.67, N 9.85%; found: C 84.53, H 5.76, N 9.94%. M. pt > 300 ºC.

Synthesis of [4-(OH)-(C$_6$H$_4$)$_2$-3,5-(CH)$_2$]$_2$[CH$_2$CH$_2$(2-C$_6$H$_4$N)$_2$]$_4$·0.5MeCN·5DMF (3)

4,4'-Dihydroxy-[1,1'-biphenyl]-3,3',5,5'-tetracarbaldehyde (596.5 mg, 2.0 mmol) and 2 equivalents of 2,2'-ethylenedianiline (849.2 mg, 4.0 mmol) were reacted in 50 mL toluene with adding 3 drops of formic acid. After drying and washing with acetonitrile, the residue was refluxed in toluene (30 mL) with 6 equivalents of CoBr$_2$ (1.312 g, 6 mmol) for 12 h. Removal of volatiles *in-vacuo*, followed by recrystallization from hot DMF (20 mL) affording orange crystals. Yield (452 mg, 26.8%). IR (KBr, cm^{-1}): 3440 (m), 2954 (s), 2922 (s), 2854 (s), 2726 (w), 2671 (w), 1661 (w), 1621 (m), 1588 (m), 1571 (m), 1461 (s), 1377 (s), 1261 (s), 1210 (m), 1154 (m), 1088 (m), 1018 (m), 873 (m), 800 (s), 750 (s), 722 (m), 671 (w). MS (ES$^+$): C$_{88}$H$_{68}$N$_8$O$_4$ (sample dried *in-vacuo*) 1301.7. Elemental analysis calculated for C$_{103}$H$_{103}$N$_{13}$O$_9$: C 74.21, H 6.23, N 10.92%; found: C 74.33, H 6.30, N 10.99%. M. pt > 300 ºC.

Synthesis of Pd@Schiff base composite

Pd(OAc)$_2$ (0.225 g, 1.0 mmol) was added to **2** [C$_6$H$_3$-1,3,5-(CH)]$_2$[CH$_2$CH$_2$(2-C$_6$H$_4$N)$_2$]$_3$ (0.924 g, 1.0 mmol) in the presence of Et$_3$N (0.14 mL, 1.0 mmol)) in 30 mL methanol. The system was stirred overnight at room temperature, then the solvent was removed affording the Pd@Schiff base composite. PXRD, SEM, XPS, together with TEM were used for the characterization of the as-prepared composite.

Experiments of peroxidase mimic activity

To evaluate the peroxidase-like activity of the synthesized composite, 60 µL of 3,3',5,5'-tetramethylbenzidine TMB (25 mM) and 20 µL of H_2O_2 (0.1M) were added in 100 mM NaAc-HAc buffer (pH=4.0) in the presence of Pd@Schiff base catalyst (0.5 mg), and the total volume of the solution was made to 3 mL. UV-vis spectra were used to detect the absorbance change at 652 nm to detect the oxidation of TMB. The peroxidase-like activity experiments were carried out under room temperature unless stated otherwise. Experiments were repeated three times to obtain the average value.

Antibacterial studies

Escherichia coli and *Staphylococcus aureus* were propagated in a Luria−Bertani (LB) or mueller hinton broth, respectively, at 37 °C under 200 rpm shaking overnight. The bacteria were gently detached from the agar plate using a sterilized loop, then incubated at 37 °C with media overnight. Then 0.5 mL of the grown *E. coli* or *S. aureus* culture was incubated at 37 ºC for 24h with 10 mL of LB. Then 10 µL of bacterial solution, 40 µL of NaAc-HAc buffer (pH=4.0), 40 µL of Pd@Schiff base material, 40 µL of 0.5 mM H_2O_2 together with 270 µL of DMEM were incubated at 37 °C for 12 h. The samples were successively diluted 8 times, and then 10 µL of each sample was placed on an agar plate and cultured for 12h to observe the number of bacterial colonies. The antibacterial activities of the Pd@Schiff base were evaluated using the colony forming unit counting method. Experiments for the Pd@Schiff base material only, and the H_2O_2 only system were also carried out as a control in order to illustrate the antibacterial activity of the as prepared Pd composite.

Experiments were repeated three times to obtain the average value.

RESULTS AND DISCUSSION

Structures of the double-layered macrocycles

The double-layer [2+2] macrocycle **1** was synthesized in good yield (*ca*. 70%) via a one-step solvent-mixing method. The reaction of 4,4'-biphenyldicarboxaldehyde with one equivalent of 2,2'-ethylenedianiline at room temperature in the presence of trifluoroacetic acid (Scheme 1) afforded the [2+2] structure (Scheme 2). The double layer [2+2] macrocycle was characterized by multinuclear ^{1}H NMR and FT-IR spectroscopy, elementary analysis, ESI-MS analyses and by single crystal X-ray diffraction. The formation of [2+2] assembled molecule was unambiguously established by the peak at m/z =773.4 corresponding to [M+H]$^+$ in the ESI-MS spectrum (Figure S1, ESI). Small single crystals suitable for X-ray diffraction using synchrotron radiation were grown from a saturated toluene/CH_2Cl_2 solution (1:1) at room temperature. Various views of the molecular structure are shown in Figure 1. The [2+2] macrocycle crystallizes in the centrosymmetric space group *P2$_1$/c* with two symmetry-unique molecules in the asymmetric unit that are related by a pseudo-translation of *b/2*. The molecular conformation of the two molecules is very similar; these differ only in the conformation of one -CH_2CH_2- link. There is simple primitive packing of these pairs of molecules according to the space group symmetry. No classical hydrogen bonds are present but there are numerous C–H···π interactions connecting neighbouring macrocycles as shown in Figure 1b. Alternative views of **1** are provided in the SI (Figures S2 and S3), the asymmetric unit is shown in Fig. S4, and the overlap of the two chemically identical molecules of **1** is given in Fig. S5.

By treating 1,3,5-triformylbenzene with 2,2'-ethyenedianiline in a 2:3 stoichiometric ratio in dichloromethane, in the presence of trifluoroacetic acid, a [2+3] double layer macrocycle **2** was isolated. The [2+3] macrocycle is enthalpically favoured because of the lesser angle strain and is entropically favoured due to it been comprised of the minimum number of building blocks

compared to all the possible 3D architectures.[26] The [2+3] macrocycle was characterized by multinuclear NMR (^{1}H, ^{13}C), ^{1}H-^{1}H COSY, HBMC and FT-IR spectroscopy, elemental
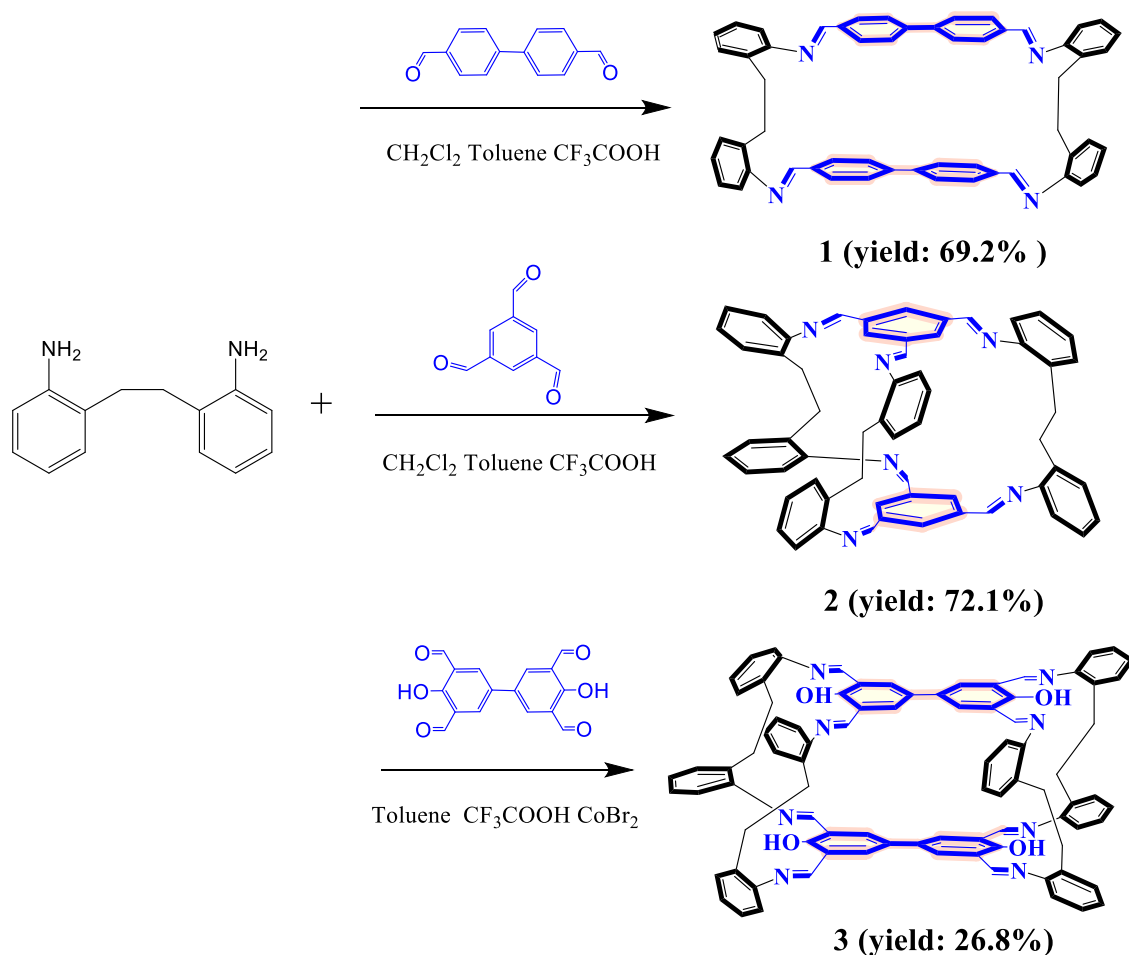
Scheme 1. Preparation of **1 – 3**.

analysis and ESI-MS analyses (Figures S6-S10, SI). Single crystals suitable for X-ray diffraction were grown from a saturated dichloromethane solution at room temperature. Various views of the molecular structure are shown in Figure 2. The [2+3] macrocycle crystallizes in the centrosymmetric space group *Pbca* with a single macrocycle and one dichloromethane in the asymmetric unit.
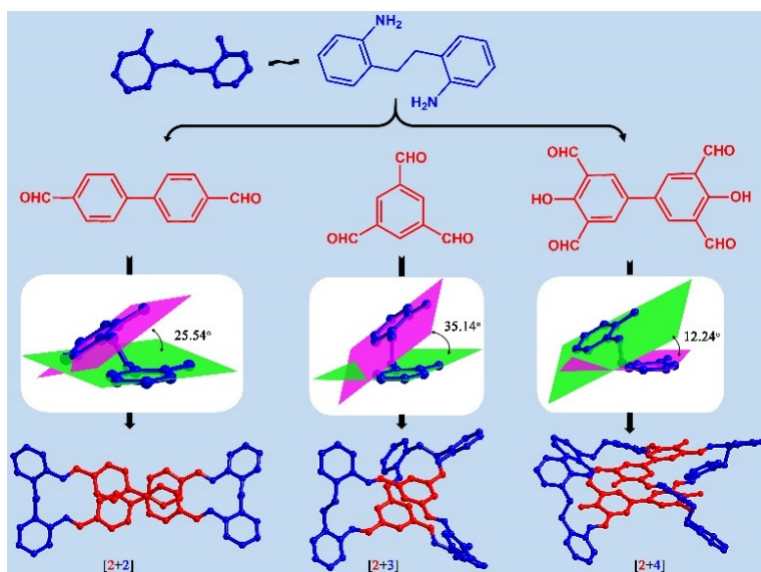
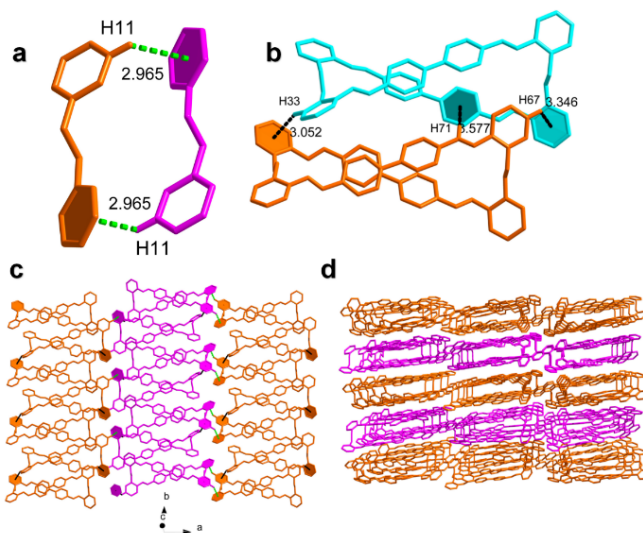**Scheme 2.** Crystal Structure for [2+2] (**1**), [2+3] (**2**) and [2+4] (**3**) macrocycles.

Figure 1. Structure of the [2+2] macrocycle **1**. a) and b) C-H···π interactions; c) the 2D network linked via the C-H···π interactions; d) 3D packing pictures for [2+2] macrocycle.
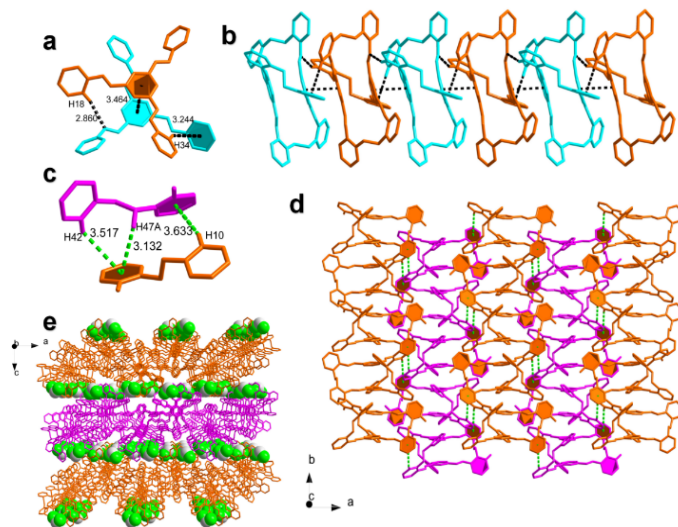
Figure 2. Structure of the [2+3] macrocycle **2**. (a) C-H···π and π···π interactions; b) The 1D chain along [010]; c) C-H···π and π···π between molecules; d) 2D network linked via the C-H···π interactions; e) packing of the [2+3] macrocycle with CH_2Cl_2 between macrocyclic molecules.

The molecules are arranged in columns parallel to the crystallographic *b*-axis (Figure 2b) with numerous C–H···π interactions and π···π interactions connecting neighboring macrocycles (Figures 2a-2d). The dichloromethane molecules appear to reside in pockets between macrocyclic molecules (Figure 2e) rather than in channels. There are C–H···π and C-H···Cl interactions between the dichloromethane and surrounding macrocycles. Alternative views of **2** are provided in the SI (Figures S11 and S12); the asymmetric unit is given in Fig. S13. The peak at m/z =853.4 in the ESI-MS spectrum (Figure S14, SI) confirms the formation of the double layer macrocycle.

In the case of the [2+4] macrocycle **3**, it proved necessary to employ a two-step procedure. Firstly, 4,4'-dihydroxy-[1,1'-biphenyl]-3,3',5,5'-tetracarbaldehyde and two equivalents of 2,2'-

11

ethylenedianiline were refluxed in toluene in the presence of formic acid. After the toluene was removed and the residue washed using acetonitrile, the system was refluxed in toluene again with 6 equivalents of $CoBr_2$ (note $ZnBr_2$ or $FeBr_2$ can also be employed), affording after work-up (recrystallization from hot DMF), a red crystalline solid. The limited solubility of this macrocycle prevented characterization by NMR spectroscopy, however, FT-IR spectroscopy, elementary analysis and ESI-MS analyses were possible. Moreover, single crystals suitable for X-ray diffraction were grown from a saturated DMF solution at room temperature. Various views of the molecular structure are shown in Figure 3. Alternative views of **3** are provided in the SI (Figures S15 and S16); the asymmetric unit is given in Fig. S17.
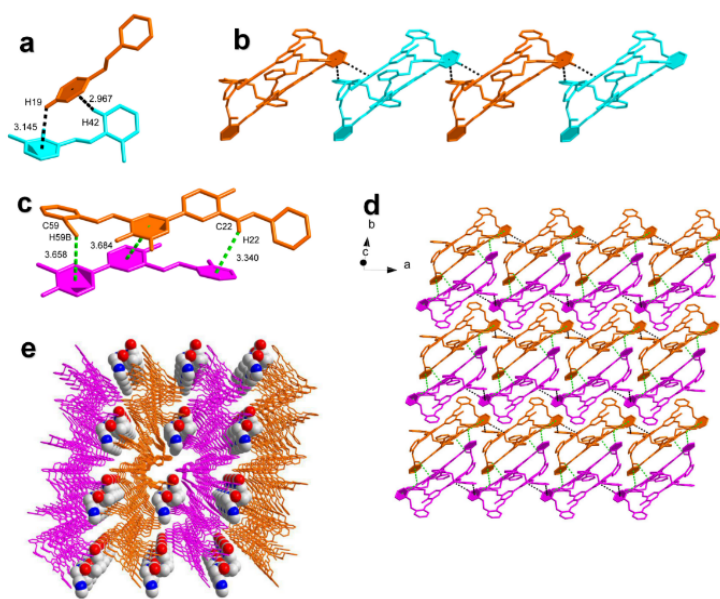

Figure 3. Structure of the [2+4] macrocycle **3**. (a) C-H···π interactions between molecules; b) 1D chain by non-covalent interactions along [010]; c) C-H···π and π ···π interactions between neighboring macrocycles; d) the 2D network linked via the C-H···π interactions; e) packing of the [2+4] macrocycle with DMF between macrocyclic molecules.

This large macrocycle crystallizes in the centrosymmetric space group *P-1* with a single macrocycle and five DMF molecules and one MeCN in the asymmetric unit. The solid-state structure helps to define the topology of this macrocycle; if the 3-connected aromatic rings are taken as nodes, then this molecule is seen as a tetrahedron. There are intermolecular O-H⋯N hydrogen bonds present and as for the [2+3] structure, C–H⋯π interactions and π⋯π interactions were found between neighboring macrocycles (Figure 4a); DMF molecules were found to be present in the intermolecular spaces (Figure 4e).

Macrocycles **1**-**3** are stable in solution following heating in toluene for 48h (no changes in NMR and/or IR spectra were observed) or on prolonged standing (1 week) in either toluene (for **1** and **2**) or DMF (for **3**).
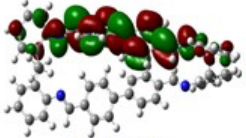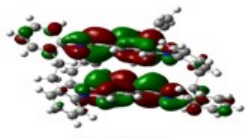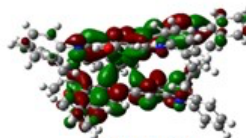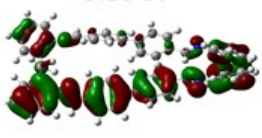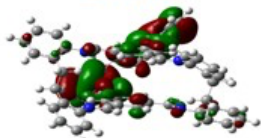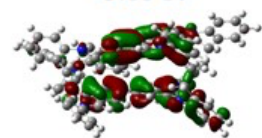

DFT studies on the double layer macrocycles

In order to discuss the electron distribution of the double layer Schiff base macrocycles, density function theory (DFT) calculations at the RB3LYP/6-311G(d,p) level were carried out using a Gaussion 09 program. The energy gap (E_g) is 3.54 eV for [2+2] macrocycle (**1**), 3.81 eV for [2+3] macrocycle (**2**) and, 3.18 eV [2+4] macrocycle for **3**, respectively.

The different electronic structures and energy levels lead to the differences in the electronic spectra between those compounds. The optimized molecular structures and the corresponding HOMO-LUMO levels are shown in Table 1 using the single-crystal structure as a model. For the [2+2] structure **1**, the HOMO and LUMO levels are separated on two diphenyl rings groups, respectively, whilst the HOMO and LUMO energy level of the [2+3] structure **2** is only centralized on the salicylaldehyde groups. In the [2+4] macrocycle **3**, the HOMO and LUMO level are mostly localized on the salicylaldehyde and a bridging imine group. The difference in the electronic distribution may be due to the presence of the charge delocalization of the six-

membered ring consisting of intramolecular hydrogen bonds formed by O atoms, hydrogen atoms and adjacent N atoms in **3**. Compared to **2**, the intramolecular H-bonding in **3** and the extended π-conjugation in **2** could enhance the HOMO energy level and lower the LUMO energy level.

Table 1. HOMO/LOMO orbitals and energy level for the macrocycles **1**-**3**. Optimized geometry and electronic distribution of the frontier for the macrocycles

	2+2	2+3	2+4
LUMO	-2.31 eV	-2.20 eV	-2.45 eV
ΔE_g	3.54	3.81	3.18
HOMO	-5.85 eV	-6.01 eV	-5.63 eV

Preparation and characterization of Pd@Schiff base

The [2+3] macrocycle was chosen for the incorporation Pd because of its high yield and facile synthesis. As can be seen from Figure 4a, in the PXRD pattern, the diffraction peaks at $2\theta =$ 40.0, 46.6, 68.4° can be assigned to the (111), (200), (220) reflections of the Pd metallic phase, consistent with the successfully immobilization of the Pd. Moreover, SEM was used to study the morphology of the Pd@Schiff base and this is exhibited in Figure 4. Figure 4b reveals the rod-like morphology of the [2+3] macrocycle; the SEM image of Pd@Schiff base composite is depicted in Figure 4c. The SEM elemental mappings further illustrate that Pd is uniformly

distributed over the Schiff base structure (Figure 4d). Transmission electron microscope (TEM) was used to investigate the morphology of the as-prepared nanoparticle composites. Figure 5 reveals that the Pd nanoparticles are highly dispersed on the Schiff base macrocycle with a well-formed crystalline structure. The size of the Pd nanoparticles was measured using TEM micrographs and the corresponding size distribution of the immobilized Pd nanoparticles are displayed in Figure 5. The average size distribution is 2.7 ± 0.8 nm, which is uniform and much smaller than in other Pd composites, for example, Pd/GO nanocomposite (5-10 nm),[27] palladium nanoparticle-loaded carbon nanofibers (73 nm),[28] Pd NPs-C60 (10.5 nm).[29] Apparently, smaller Pd nanoparticles can be beneficial to both the surface area and catalytic ability of the Pd@Schiff base composite.[27] The lattice spacings of 2.285 and 1.979 Å shown in Figure 5c can be assigned to {111} and {200} lattice planes of the Pd NPs. The IR spectrum was recorded before and after immobilization, and no significant change was found, illustrating the stability of the [2+3] macrocycle during the Pd immobilization (Figure S18, SI).
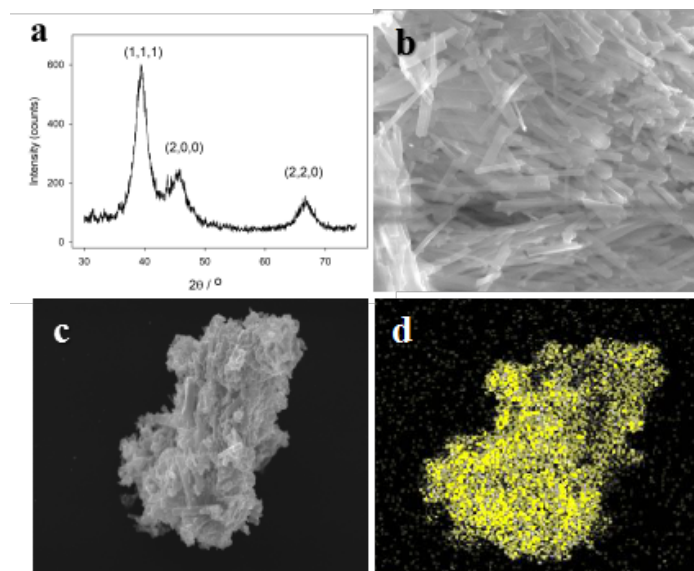
Figure 4. a) PXRD of the Pd@Schiff base product; b) SEM of the [2+3] macrocycle; c) SEM of the Pd@Schiff base composite; d) Pd mapping for the Pd@Schiff base composite.
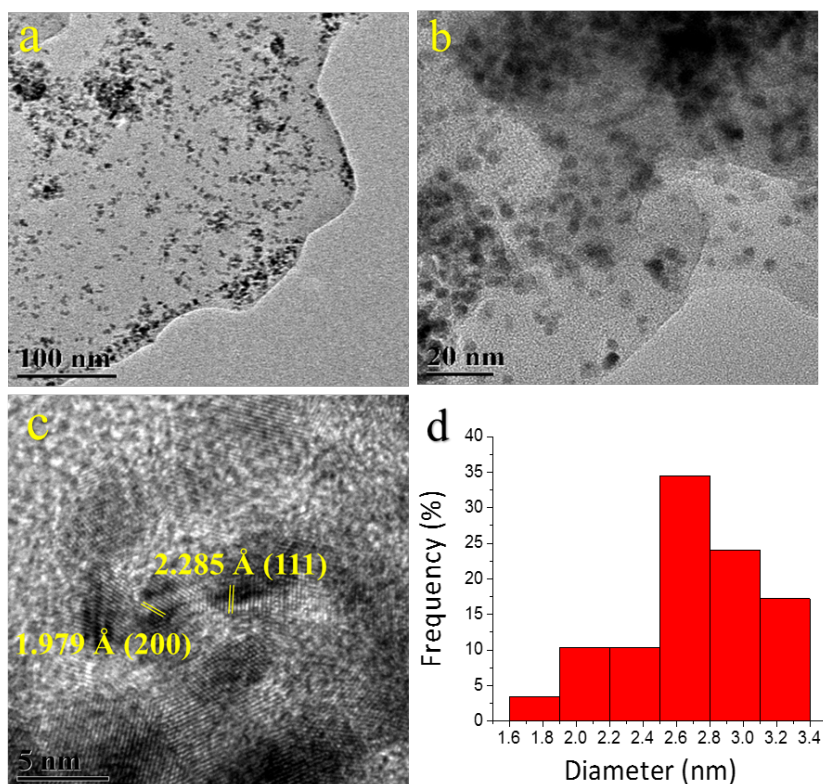

Figure 5. TEM micrographs a-c) with their d) corresponding size distribution histograms.

X-ray photoelectron spectroscopy (XPS) was carried out to investigate the nature of the Pd in the composite. Figure S19 (SI) shows the (a) XPS survey spectrum (a) and (b) Pd 3d spectrum. For the composite sample, the major component is the Pd(0) state with a binding energy of 334.2 eV and 339.4 eV for $3d_{5/2}$ and $3d_{3/2}$, respectively. There are also some smaller peaks corresponding to binding energies of 337.62, 336.4 eV and 34.2.6 eV, which may be ascribed to a small amount of absorbed Pd^{2+} ions or oxidized Pd species.[30]

Peroxidase-like activity of Pd@Schiff base

The peroxidase-like catalytic activity of the Pd@Schiff base composite was investigated via the oxidation of 3,3',5,5'-tetramethylbenzidine (TMB) in the presence of H_2O_2. Hydrogen peroxide can oxidize TMB in the presence of the Pd@Schiff base composite forming a blue colored product (oxTMB) and exhibits an absorption at 652 nm. As shown in Figure 6, the colour change can only be observed in the Pd@Schiff-base-TMB -H_2O_2 system, whereas, by contrast, no oxidation was evident in the Pd@Schiff base-TMB system, Pd@Schiff base leaching solution- TMB-H_2O_2 system or TMB-H_2O_2 system, reveals that the peroxidase-like activity of our synthesized Pd@Schiff base composite.

The pH conditions for the peroxidase-like activity of Pd@Schiff base were optimized as shown in Figure S20, SI. The pH played an important role in the catalytic process, and the Pd@Schiff base was not active under alkaline conditions, whilst pH = 4 was found to be the optimum. In addition, the effect of temperature was also addressed, and the peroxidase-like properties were found to be enhanced as the temperature increased from room temperature (15 ℃) to 60 ℃.
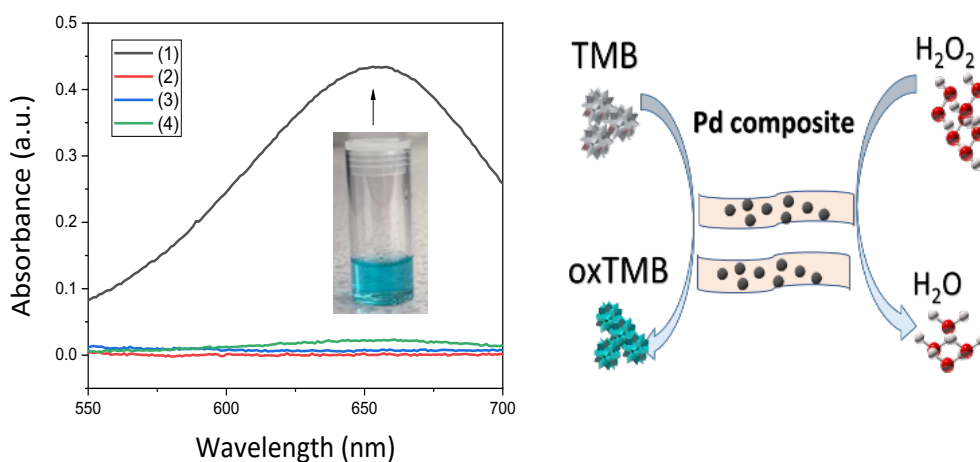
Figure 6. Absorbance spectra of oxTMB in different reaction conditions: 1) Pd@Schiff base + TMB + H_2O_2; 2) Pd@Schiff base + TMB; 3) Pd@Schiff base leaching solution + TMB + H_2O_2; 4) TMB + H_2O_2.

Table 2. Kinetic parameters of HRP and other Pd based peroxidase mimetics using TMB as substrate.

Catalyst	K_m (mM)		V_{max} (10^{-8} $M \cdot s^{-1}$)		Reference
	H_2O_2	TMB	H_2O_2	TMB	
HRP	3.7	0.43	8.71	10.00	2
MoS_2-PPy-Pd	6.4	0.93	-	-	32
$Fe_3O_4@SiO_2$-NH_2-Au@$Pd_{0.3}$	3.5	0.090	6.76	11.20	33
$Pd_1Cu_{1.7}$ NAFs	7.782	0.377	69.04	53.24	34
Pd NAFs	13.768	0.040	29.06	16.89	35
Pd@Schiff base	1.17	8.86	3.67	3.72	This work

Kinetic studies

Steady-state kinetic measurements were carried out to evaluate the kinetic process of the peroxidase-like activity of the Pd@Schiff base composite. The oxidation process follows the "ping–pong" mechanism given the the double reciprocal plot is near linear (Figures S21c and d, SI).[31] The calculated K_m and V_{max} values for the Pd@Schiff base toward H_2O_2 and TMB are shown in Table 2. The synthesized Pd@Schiff base composite possesses relatively small K_m values illustrating the favorable combination with H_2O_2 and their potential as peroxidase-like mimetics.

Antibacterial studies

A number of the peroxidase-like mimetics have been found to counter bacterial infections.[12, 35] Herein, the as-prepared Pd immobilized Schiff base composite was screened, in the presence of H_2O_2, against *E. coli* (Gram-negative bacterium *Escherichia coli*) and *S. aureus* (Gram-positive bacterium *Staphylococcus aureus*). Scanning electron microscopy (SEM) was used to examine the change of bacteria morphology after being treated by Pd@Schiff base/H_2O_2. As shown in Figure 7 (bottom), untreated *E. coli* cells exhibited a rod-like shape and *S. aureus* cells were more spherically shaped, whereas, after been treated with both H_2O_2 and Pd@Schiff base composite, many remarkable defects were found on the rod-like shape of *E. coli* cells and some of the *S. aureus* cells are completely destroyed. Noteworthy, the survival rates in the presence of the Pd@Schiff base composite (25 mg/L) and 50 μM H_2O_2 for the *E. coli* and *S. aureus* were
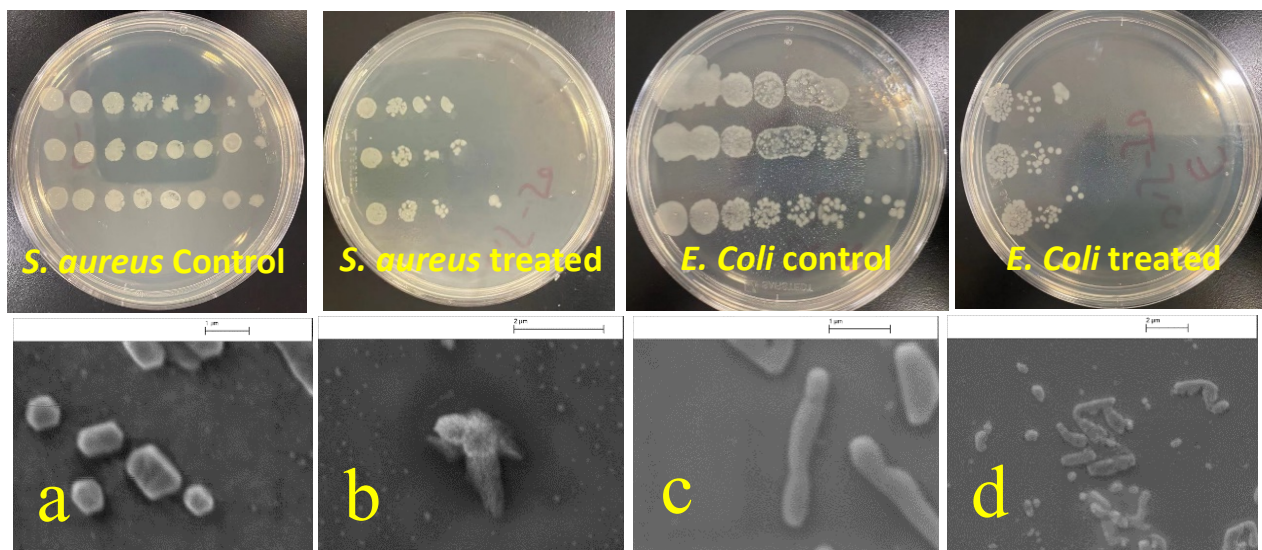
Figure 7. Agar plate for treated (25 mg/L Pd composite + 50 μM H_2O_2) and control group of *E. coli* and *S. aureus* cell lines and typical SEM images of *S. aureus* and *E. coli* cells exposed to various treatments. a) *S. aureus* control b) *S. aureus* treated with Pd@Schiff base composite and H_2O_2 c) *E. coli* control d) *E. coli* treated with Pd@Schiff base composite and H_2O_2.

Figure 8. Antibacterial efficiency towards *E. coli* and *S. aureus* for different conditions. (Experiments were repeated three times to obtain the average value).

found to be 0.00031% and 0.0316%, respectively. By contrast, without the use of the Pd@Schiff base peroxidase-like mimetic, the survival rate was increased to 25.0% and 28.6%, respectively. The antibacterial efficiency towards *E. coli* and *S. aureus* are shown in Figure 8. The Pd composite exhibited better bacterial performance than the antibiotic ciprofloxacin;[37] using the same concentration, the survival rate using ciprofloxacin is 9.28% and 10.0 % for *E. coli* cells and *S. aureus* cells, respectively.[38] These results illustrated that use of H_2O_2 combined with Pd@Schiff base composite exerts strong antibacterial activity against both *S. aureus* and *E. coli*.

Cytotoxicity studies

In order to evaluate the biocompatibility of the as-prepared Pd@Schiff base composite, cytotoxicity tests were carried out against HaCaT and Hep-G2 cell lines using the MTS assay (Figure S22, SI). In summary, cell cultures were treated with of Pd@Schiff base composite; Pd@Schiff base and H_2O_2 incubated for 24 h at 37 °C in a 5% CO_2 incubator. After work up with MTS, the absorbance was measured using a microplate reader at a wavelength of 490 nm. A calibration curve was first plotted on different set amount of HaCaT cells *versus* absorbance at 490 nm. MTS graphs for treatment of HaCaT and Hep-G2 using the Pd composite are shown in Figure S23, SI. Bright-field microscopy images and fluorescence microscopy images of the HaCaT and Hep-G2 cells under different conditions are shown in Figures S24 and S25, SI. The result shows that the synthesized Pd is non-toxic even at high concentrations, given the viability of cells are almost unchanged on the addition of hydrogen peroxide.

Conclusions

In conclusion, three new [2+2] [2+3] and [2+4] double layer Schiff-base macrocycles derived from condensation reactions involving 2,2'-ethylenedianiline and di-, tri- or tetra-aldehydes have been synthesized and structurally characterized. The [2+3] derivative formed a composite with Pd and was used as a horseradish peroxidase mimetic. When the reaction pH was 4.0, the system exhibited the highest absorbance at 652 nm, indicating optimum catalytic activity. From the kinetic studies, the peroxidase-like activity of the Pd@Schiff base composite exhibited Michaelis−Menten type kinetics and a "ping−pong" mechanism. By utilizing the peroxidase mimic activity of the Pd composite, an antibacterial system of Pd@Schiff base together with a low concentration of H_2O_2 was established and the sterilization rate can reach over 99% towards both *E. coli* and *S. aureus* under optimized conditions. In addition, the Pd@Schiff base material exhibited a

satisfactory biocompatibility level towards HaCaT and Hep-G2 cell lines. This work provides a new composite which can behave as an enzyme-like mimetic and exhibits antibacterial properties. The work will guide the development of new composite-based therapies for bacterial infections.

ASSOCIATED CONTENT

Supporting Information.

  1) experimental procedure,

  2) Characterizations of Schiff base macrocycles and Pd composites,

  3) Asymmetric unit of double-layer Schiff-base macrocycles,

  4) MTS graph for Pd@Schiff base against HaCaT and Hep-G2 cells,

  5) The optimum conditions together with the catalytic kinetics of the enzyme-like activity,

  6) Crystallographic data are provided in the SI.†

AUTHOR INFORMATION

Corresponding Author

*Carl Redshaw – Department of Chemistry, University of Hull, Hull, HU6 7RX, U.K. orcid.org/0000-0002-2090-1688 Email. C.Redshaw@hull.ac.uk

Authors

Kuiyuan Wang – Department of Chemistry, University of Hull, Hull, HU6 7RX, U.K. orcid.org/0000-0001-9604-7898

Kai Chen – School of Environmental Science and Engineering, Nanjing University of Information Science & Technology, Nanjing 210044, P. R. China. orcid.org/0000-0002-5852-3264

Timothy J. Prior – Department of Chemistry, University of Hull, Hull, HU6 7RX, U.K.

Xing Feng - School of Materials and Energy, Guangdong University of Technology, Guangzhou, Guangdong 510006, People's Republic of China.

Author Contributions

Kuiyuan Wang: Investigation; Writing. Kai Chen: Drawing crystal structure; TEM and XPS test and analysis; Timothy J. Prior: Refinement of single crystal structures, discussion about the macrocycle structures. Xing Feng: DFT studies. Carl Redshaw: Funding acquisition; Supervision; Writing, review & editing.

Funding Sources

ACKNOWLEDGMENT

ABBREVIATIONS
TMB: 3,3',5,5'-tetramethylbenzidine.
BRIEFS: Antibacterial performance and peroxidase mimic activity of Pd immobilized Schiff-base double layer macrocycle.

Author Contributions

Kuiyuan Wang: Investigation; Writing. Kai Chen: Drawing crystal structure; TEM and XPS test and analysis; Timothy J. Prior: Refinement of single crystal structures, discussion about the macrocycle structures. Xing Feng: DFT studies. Carl Redshaw: Funding acquisition; Supervision; Writing, review & editing.

Conflicts of interest

There are no conflicts to declare.

Notes and references

NOTES

CCDC 2076122-2076124 contain the supplementary crystallographic data for 1-3. These data can be obtained free of charge via http://www.ccdc.cam.ac.uk/conts/retrieving.html or from the Cambridge Crystallographic Data Centre, 12 Union Road, Cambridge, CB2 1EZ, UK; fax (+44) 1223-336-033; or e-mail: deposit@ccdc.cam.ac.uk.

REFERENCES

[1] Underkofler, L. A.; Barton, R. R.; Rennert, S. S. Production of Microbial Enzymes and Their Applications. Appl. Microbiol., 1958, 6, 212–221.

[2] Wang, K.; Song, J.; Duan, X.; Mu, J.; Wang, Y. Perovskite $LaCoO_3$ Nanoparticles as Enzyme Mimetics: Their Catalytic Properties, Mechanism and Application in Dopamine Biosensing. New J. Chem., 2017, 41, 8554–8560.

[3] Chen, Z. W.; Yin, J. J.; Zhou, Y. T.; Zhang, Y.; Song, L.; Song, M. J.; S. L. Hu, S. L.; Gu, N. Dual Enzyme-like Activities of Iron Oxide Nanoparticles and Their Implication for

Diminishing Cytotoxicity. ACS Nano 2012, 6, 4001–4012.

[4] Lewandowski, L.; Kepinska, M.; Milnerowicz, H. The Copper-Zinc Superoxide Dismutase Activity in Selected Diseases. Eur. J. Clin. Invest. 2019, 49, e13036.

[5] Youngjun, L.; Devaraj, N. K. Lipase Mimetic Cyclodextrins. Chem. Sci. 2021, 12, 1090–1094.

[6] Gao, L. Z.; Zhuang, J.; Nie, L.; Zhang, J. B.; Zhang, Y.; Gu, N.; Wang, T. H.; Feng, J.; Yang, D. L.; Perrett, S.; Yan, X. Intrinsic Peroxidase-Like Activity of Ferromagnetic Nanoparticles. Nat. Nanotechnol. 2007, 2, 577–583.

[7] Hu, Y.; Cheng, H.; Zhao, X.; Wu, J.; Muhammad, F.; Lin, S.; He, J.; Zhou, L.; Zhang, C.; Deng, Y.; Wang, P.; Zhou, Z.; Nie, S.; Wei, H. Surface-Enhanced Raman Scattering Active Gold Nanoparticles with Enzyme-Mimicking Activities for Measuring Glucose and Lactate in Living Tissues. ACS Nano 2017, 11, 5558–5566.

[8] Singh, V. K.; Yadav, P. K.; Chandra, S.; Bano, D.; Talat, M.; Hasan, S. H. Peroxidase Mimetic Activity of Fluorescent NS-Carbon Quantum Dots and Their Application in Colorimetric Detection of H_2O_2 and Glutathione in Human Blood Serum. J. Mater. Chem. B, 2018, 6, 5256–5268.

[9] Zhang, J. W.; Zhang, H. T.; Du, Z. Y.; Wang, X.; Yun, S. H.; Jiang H. L. Water-Stable Metal–Organic Frameworks with Intrinsic Peroxidase-Like Catalytic Activity as a Colorimetric Biosensing Platform. Chem. Commun. 2014, 50, 1092–1094.

[10] Zhang, T.; Xing, Y.; Song, Y.; Gu, Y.; Yan, X.; Lu, N.; Liu, H.; Xu, Z.; Xu, H.; Zhang, Z.; Yang, M. AuPt/MOF–Graphene: A Synergistic Catalyst with Surprisingly High Peroxidase-Like Activity and Its Application for H_2O_2 Detection. Anal. Chem. 2019, 91, 10589–10595.

[11] Wang, J.; Hu, Y. Y.; Zhou, Q.; Hu, L. Z.; Fu, W. S.; Wang, Y. Peroxidase-like Activity of Metal–Organic Framework [Cu(PDA)(DMF)] and Its Application for Colorimetric Detection of

Dopamine. ACS Appl. Mater. Interfaces 2019, 11, 44466–44473.

[12] Ge, C.; Wu, R.; Chong, Y.; Fang, G.; Jiang, X.; Pan, Y.; Chen, C.; Yin, J. -J. Synthesis of Pt Hollow Nanodendrites with Enhanced Peroxidase-Like Activity against Bacterial Infections: Implication for Wound Healing. Adv. Funct. Mater. 2018, 28, 1801484.

[13] Chen, Q. M.; Zhang, X. D.; Li, S. Q.; Tan, J. K.; Xu, C. J.; Huang, Y. M. MOF-Derived Co_3O_4@Co-Fe Oxide Double-Shelled Nanocages as Multi-Functional Specific Peroxidase-Like Nanozyme Catalysts for Chemo/Biosensing and Dye Degradation. Chem. Eng. J. 2020, 395, 125130.

[14] Yoon, T. P.; Jacobsen, E. N. Privileged Chiral Catalysts. Science 2003, 299, 1691–1693.

[15] Choi, Y. W.; Park, G. J.; Na, Y. J.; Jo, H. Y.; Lee, S. A.; You, G. R.; Kim, C. A Single Schiff Base Molecule for Recognizing Multiple Metal Ions: A Fluorescence Sensor for Zn(II) and Al(III) and Colorimetric Sensor for Fe(II) and Fe(III). Sens. Actuators, B 2014, 194, 343–352.

[16] Li, S.; Pei, M.; Wan, T.; Yang, H.; Gu, S.; Tao, Y.; Liu, X.; Zhou, Y.; Xu, W.; Xiao, P. Self-Healing Hyaluronic Acid Hydrogels Based on Dynamic Schiff Base Linkages as Biomaterials. Carbohyd. Polym. 2020, 250, 116922.

[17] Wang, K.; Prior, T. J.; Redshaw C. Turning on ROP Activity in a Bimetallic Co/Zn Complex Supported by a [2+2] Schiff-base Macrocycle. Chem. Commun. 2019, 55, 11279–11282.

[18] Yu, Q.; Zhang, X.; Wu, S. T.; Chen, H.; Zhang, Q. L.; Xu, H.; Huang, Y. L.; Zhu, B. X.; Ni, X. L. Twisted Schiff-base Macrocycle Showing Excited-State Intramolecular Proton-Transfer (ESIPT): Assembly and Sensing Properties. Chem. Commun. 2020, 56, 2304–2307.

[19] Wang, K.; Prior, T. J.; Hughes, D. L.; Arbaoui, A.; Redshaw, C. Coordination Chemistry of [2 + 2] Schiff-base Macrocycles Derived from the Dianilines [(2-$NH_2C_6H_4)_2$X] (X = CH_2CH_2, O): Structural Studies and ROP Capability Towards Cyclic Esters. Dalton Trans. 2021, 50, 8057–8069.

[20] Li, P.; Xu, S.; Yu, C.; Li, Z. Y.; Xu, J.; Li, Z. M.; Zou, L.; Leng, X.; Gao, S.; Liu, Z.; Liu, X.; Zhang, S. De Novo Construction of Catenanes with Dissymmetric Cages by Space-Discriminative Post-Assembly Modification. Angew. Chem., Int. Ed. 2020, 59, 7113–7121.

[21] Yang, X. P.; Jones, R. A.; Oye, M. M.; Holmes, A. L.; Wong, W. K. Near Infrared Luminescence and Supramolecular Structure of a Helical Triple-Decker Yb(III) Schiff Base Cluster. Cryst. Growth Des. 2006, 6, 2122–2125.

[22] Qiu, L.; McCaffrey, R.; Jin, Y.; Gong, Y.; Hu, Y.; Sun, H.; Park, W.; Zhang, W. Cage-Templated Synthesis of Highly Stable Palladium Nanoparticles and Their Catalytic Activities in Suzuki–Miyaura Coupling. Chem. Sci. 2018, 9, 676–680.

[23] Omidvar, A.; Jaleh, B.; Nasrollahzadeh, M. J. Preparation of the GO/Pd Nanocomposite and its Application for the Degradation of Organic Dyes in Water Colloid. Interface. Sci., 2017, 496, 44–50.

[24] Gao, S.; Liu, Y.; Wang, L.; Wang, Z.; Liu, P.; Gao, J.; Jiang, Y. Incorporation of Metals and Enzymes with Porous Imine Molecule Cages for Highly Efficient Semiheterogeneous Chemoenzymatic Catalysis. ACS Catal. 2021, 11, 5544–5553.

[25] Fang, G.; Li, W.; Shen, X.; Perez-Aguilar, J. M.; Chong, Y.; Gao, X.; Chai, Z.; Chen C.; Ge, C.; Zhou R. Differential Pd-Nanocrystal Facets Demonstrate Distinct Antibacterial Activity Against Gram-Positive and Gram-Negative Bacteria. Nat. Commun. 2018, 9, 129.

[26] Jin, Y.; Voss, B. A.; Jin, A.; Long, H.; Noble, R. D.; Zhang, W. Highly CO_2-Selective Organic Molecular Cages: What Determines the CO_2 Selectivity. J. Am. Chem. Soc. 2011, 133, 6650−6658.

[27] Li, J.; Liu, J.; Tan, G.; Jiang, J.; Peng, S.; Deng, M.; Qian, D.; Feng, Y.; Liu, Y. High-Sensitivity Paracetamol Sensor Based on Pd/Graphene Oxide Nanocomposite as an Enhanced Electrochemical Sensing Platform. Biosens. Bioelectron. 2014, 54, 468– 475.

[28] Huang, J.; Liu, Y.; Hou, H.; You, T. Simultaneous Electrochemical Determination of Dopamine, Uric acid and Ascorbic Acid using Palladium Nanoparticle-Loaded Carbon Nanofibers Modified Electrode. Biosens. Bioelectron. 2008, 24, 623– 627.

[29] Li, Z.; Zhang, J.; Zhou, Y.; Shuang, S.; Dong, C.; Choi, M. M. F. Electrodeposition of Palladium Nanoparticles on Fullerene Modified Glassy Carbon Electrode for Methane Sensing. Electrochim. Acta 2012, 76, 288–291.

[30] Wang, X.; Chen, J.; Zeng, J.; Wang, Q.; Li, Z.; Qin, R.; Wu, C.; Xie, Z.; Zheng, L. The Synergy Between Atomically Dispersed Pd and Cerium Oxide for Enhanced Catalytic Properties. Nanoscale, 2017, 9, 6643–6648.

[31] Bhakta, S.; Nayek, A.; Ro, B.; Dey, A. Induction of Enzyme-Like Peroxidase Activity in an Iron Porphyrin Complex Using Second Sphere Interactions. Inorg. Chem. 2019, 58, 2954– 2964.

[32] Gao, L. Z.; Zhuang, J.; Nie, L.; Zhang, J. B.; Zhang, Y.; Gu, N.; Wang, T. H.; Feng, J.; Yang, D. L.; Perrett, S.; Yan X. Intrinsic Peroxidase-Like Activity of Ferromagnetic Nanoparticles. Nat. Nanotechnol. 2007, 2, 577–583.

[33] Chi, M.; Zhu, Y.; Jing, L.; Wang, C.; Lu, X. Fabrication of Ternary MoS_2-Polypyrrole-Pd Nanotubes as Peroxidase Mimics with a Synergistic Effect and Their Sensitive Colorimetric Detection of L-Cysteine. Anal. Chim. Acta 2018, 1035, 146–153.

[34] Adeniyi, O.; Sicwetsha, S.; Mashazi P. Nanomagnet-Silica Nanoparticles Decorated with Au@Pd for Enhanced Peroxidase-Like Activity and Colorimetric Glucose Sensing. ACS Appl. Mater. Interfaces 2020, 12, 1973−1987.

[35] Liu, W.; Guo, J.; Chen, C.; Ni, P.; Jiang, Y.; Zhang, C.; Wang, B.; Lu, Y. Nanomagnet-Silica Nanoparticles Decorated with Au@Pd for Enhanced Peroxidase-Like Activity and Colorimetric Glucose Sensing. Microchim. Acta 2021, 188, 114–114.

[36] Wang, Y.; Chen, C.; Zhang, D.; Wang, Bifunctionalized Novel Co-V MMO Nanowires: Intrinsic Oxidase and Peroxidase Like Catalytic Activities for Antibacterial Application. J. Appl. Catal. B: Environ. 2020, 261, 118256.

[37] Wang A.; Weldrick P. J.; Madden L. A.; Paunov V. N.; Biofilm-Infected Human Clusteroid Three-Dimensional Coculture Platform to Replace Animal Models in Testing Antimicrobial Nanotechnologies. ACS Appl. Mater. Interfaces 2021, 13, 22182–22194.

[38] Banoee, M.; Seif, S.; Nazari, Z. E.; Fesharaki, P. J.; Shahverdi, H. R.; Moballegh, A.; Shahverdi A. R. ZnO Nanoparticles Enhanced Antibacterial Activity of Ciprofloxacin Against *Staphylococcus Aureus* and *Escherichia Coli.* J. Biomed. Mater. Res. Part B Appl. Biomater. 2010, 93, 557–561.

TOC: